SUPPLEMENTARY FIGURES

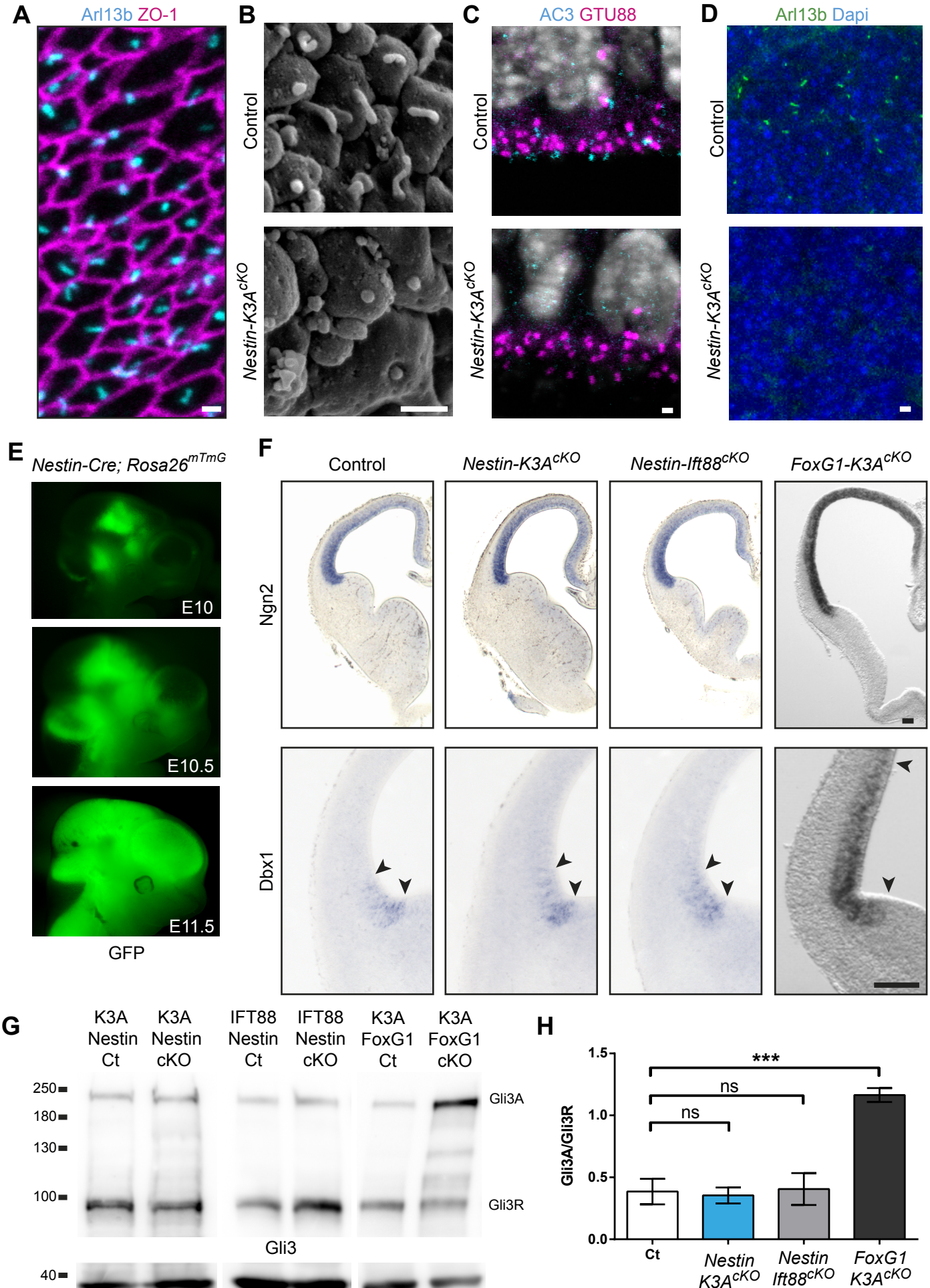

Figure S1: Patterning defects are observed in *FoxG1-cre* but not *Nestin-cre* conditional ciliary mutants. (A) Ventricular surface of the somatosensory cortex at E14.5 double immunostained with Arl13b (primary cilium, cyan) and ZO-1 (cell junctions, magenta) antibodies showing that most cells extend a primary cilium toward the ventricle. (B) Scanning electron micrographs of control and ciliary mutant cortical ventricular surfaces at E14.5 showing the absence of cilia in the mutant. (C) Double immunostaining with adenylate cyclase 3 (AC3, primary cilium, cyan) and GTU88 (pericentriolar material, magenta) antibodies counterstained with DAPI (gray) on coronal sections of the somatosensory cortex of control and *Nestin-K3A*^{cKO} mutant at E14.5 showing the apical localization of basal bodies in ciliary mutants despite the absence of cilia. (D) Immunostaining with Arl13b (green) antibody counterstained with DAPI (blue) on coronal sections of control and *Nestin-K3A*^{cKO} mutant at E14.5 showing the absence of primary cilia in the subventricular zone of the somatosensory cortex, (E) Side view of *Nestin-Cre; Rosa26*^{mTmG} at E10, E10.5 and E11.5 showing that GFP expression is induced from E11 in the telencephalon. (F) *In situ* hybridization with Ngn2 and Dbx1 probes on coronal sections of *Nestin-Ift88*^{cKO}, *Nestin-K3A*^{cKO}, *FoxG1-K3a*^{cKO} conditional mutants and controls at E12.5. Patterning defects are observed in *FoxG1-K3a*^{cKO} mutants, but not in *Nestin-K3A*^{cKO} ciliary mutants or controls. (F) Western blots of cortical lysates from *Nestin-K3A*^{cKO}, *Nestin-Ift88*^{cKO}, *FoxG1-K3a*^{cKO} mutants and their controls at E12.5. The Gli3A- and Gli3R-immunoreactive bands migrate at 190 and 83 kDa, respectively. (G) Quantification of the Gli3A:Gli3R ratio in control and ciliary mutants shows no significant differences among the genotypes except in *FoxG1-K3a*^{cKO} mice in which Gli3A is significantly more abundant compared to Gli3R. Data are the mean ± s.e.m (C). Scale bars: 1 µm in (A-D), 100 µm in (F).

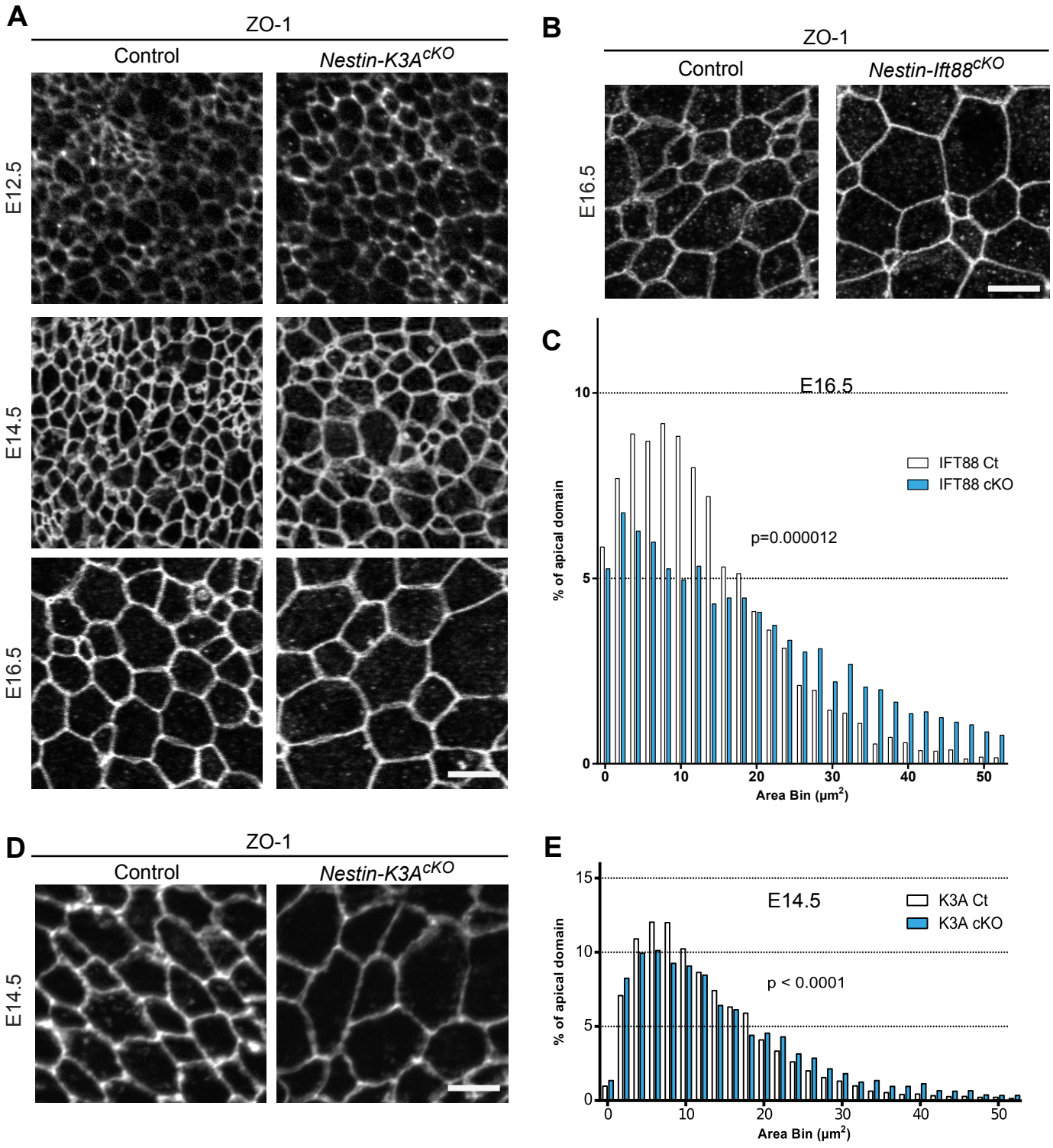

Figure S2: Cilia abrogation leads to RGC apical domain enlargement in the somatosensory cortex and in the LGE. (A) Immunostaining with ZO-1 antibody on ventricular surfaces from whole mounts of the somatosensory cortex of a control and *Nestin-K3A*^{cKO} ciliary mutant at the indicated stages. Corresponding segmented images are shown in Figure 2B. (B) Immunostaining with ZO-1 antibody on ventricular surfaces from whole mounts of control and *Nestin-Ift88*^{cKO} mice at E16.5. (C) Distribution of apical domain surfaces from control (white) and *Nestin-Ift88*^{cKO} (blue) embryos at E16.5 (2 µm^2 bins). (D) Immunostaining with the ZO-1 antibody on ventricular surfaces from whole mounts of the LGE of a control and a *Nestin-K3A*^{cKO} ciliary mutant at E14.5. (E) Distribution of apical domain surfaces of the LGE from control (white) and *Nestin-K3A*^{cKO} (blue) embryos at E14.5 (2 µm^2 bins). Scale bars: 5 µm.

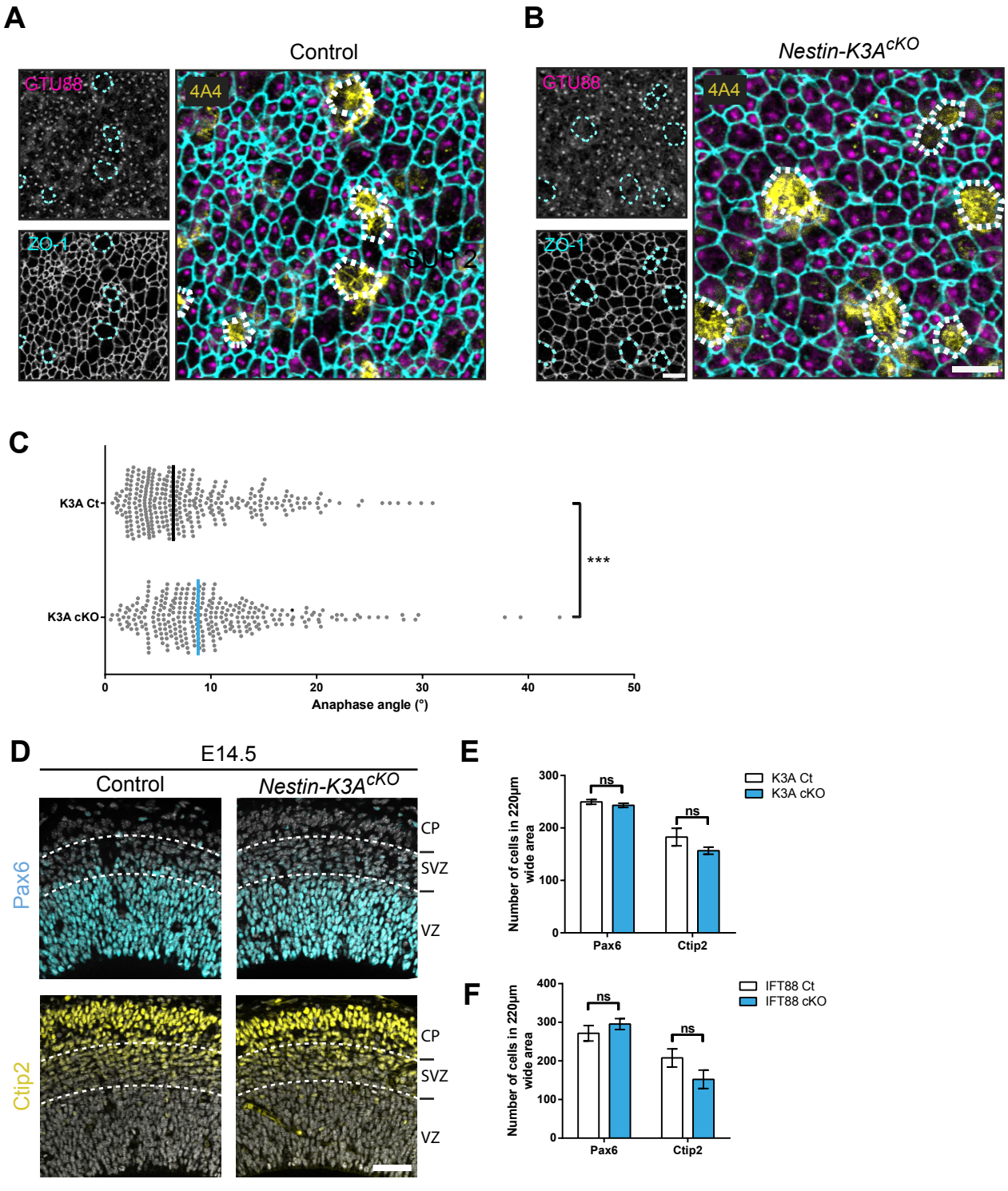

Figure S3: Characterization of cortical cell types in controls and ciliary mutants.

(A-B) Triple immunostaining with ZO-1 (cell junctions, cyan), GTU88 (pericentriolar materials, magenta) and 4A4 (mitotic cells, yellow) antibodies on whole mounts of control (A) and ciliary mutant (B) cortical ventricular walls at E14.5. Corresponding segmented images are shown in Figure 3C. Apical cell contacts of $GTU88^{-}/4A4^{+}$ mitotic cells are outlined by white dotted lines. (C) Quantification of mitotic spindle orientation at E12.5 showing a 31% increase in ciliary mutants compared to controls. Anaphase angles measured: 344 per genotype. (D) Immunostaining with Pax6 (RGC, cyan) or Ctip2 (early-differentiated neurons, yellow) antibodies on E14.5 coronal sections from a control and a $Kif3a^{cKO}$ ciliary mutant. The boundaries between the layers (ventricular zone, VZ; subventricular zone, SVZ; cortical plate, CP) are indicated by white dotted lines. (E, F) Quantification of the numbers of $Pax6^{+}$ and $Ctip2^{+}$ cells in *Nestin-K3A*^{cKO} and *Nestin-Ift88*^{cKO} mutants and their respective controls. Scale bars: 5 µm in A, B and 50 µm in D.

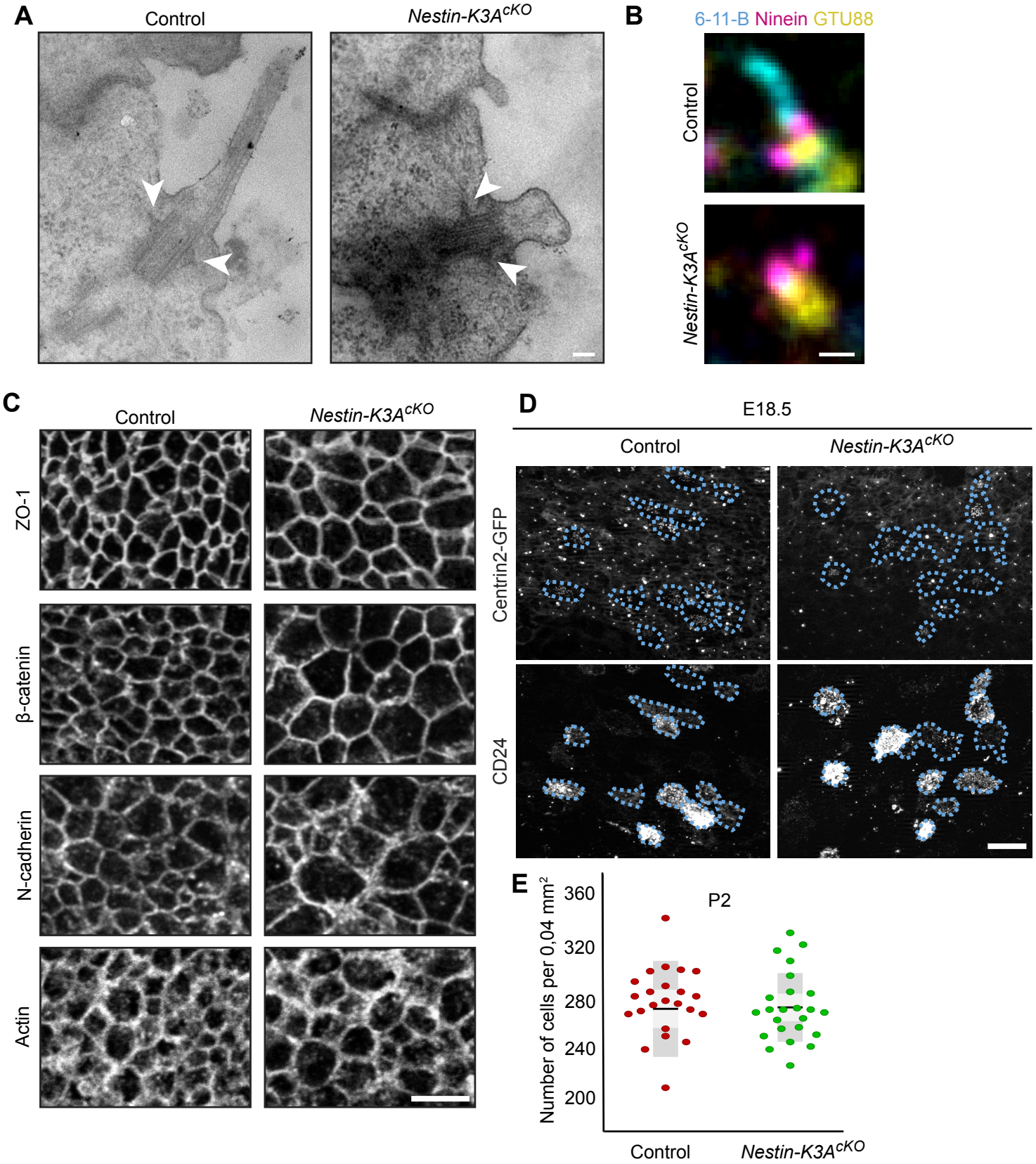

Figure S4: Depletion of the primary cilium from radial glia does not affect cell junctions, centriolar appendage formation or ependymal specification. (A) Transmission electron micrograph of control and ciliary mutant apical domains at E14.5 showing normal formation of subdistal appendages (arrowheads). (B) Triple immunostaining of E14.5 control and mutant cortical ventricular surfaces with 6-11-B (cilia, cyan), ninein (subdistal appendages, magenta) and GTU88 (pericentriolar materials, yellow) antibodies showing similar ninein staining in the control and the mutant despite depletion of primary cilia. (C) Immunostaining with ZO-1, β-catenin, N-cadherin (adherens junctions) or F-actin antibodies on E14.5 WM cortical ventricular surface shows no defects in cell junctions or actin cytoskeleton in ciliary mutants compared to controls. (D) Immunostaining with the CD24 antibody (magenta) on whole mounts of *Centrin2-GFP; Kif3a*^{cKO} mutants or *Centrin2-GFP* control cortices at E18.5; cells specified for the ependymal lineage are recognized by the multiple *Centrin2-GFP*$^{+}$ dots in the cytoplasm and circled with blue dotted lines; similar staining with the CD24 antibody and *centrin2-GFP* transgene show no premature differentiation of multiciliated ependymal cells in the ciliary mutant compared to the control. (E) Quantification of DAPI^{+} cells per 0.04 mm^{2} in the cortex of controls and ciliary mutants at P2. Scale bars: 100 µm in (A), 0.5 µm in (B), 5 µm in (C) and 50 µm in (D).

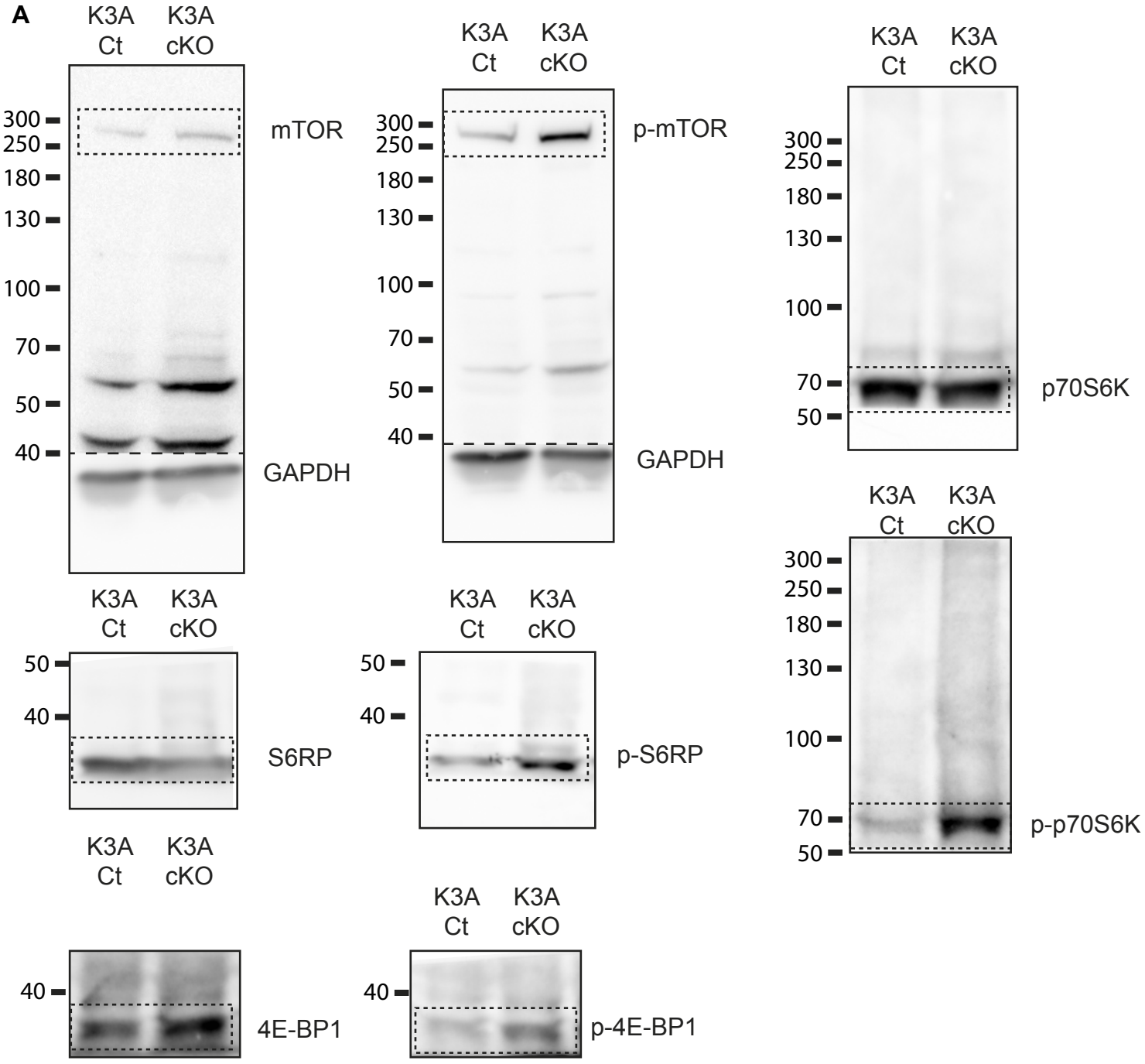

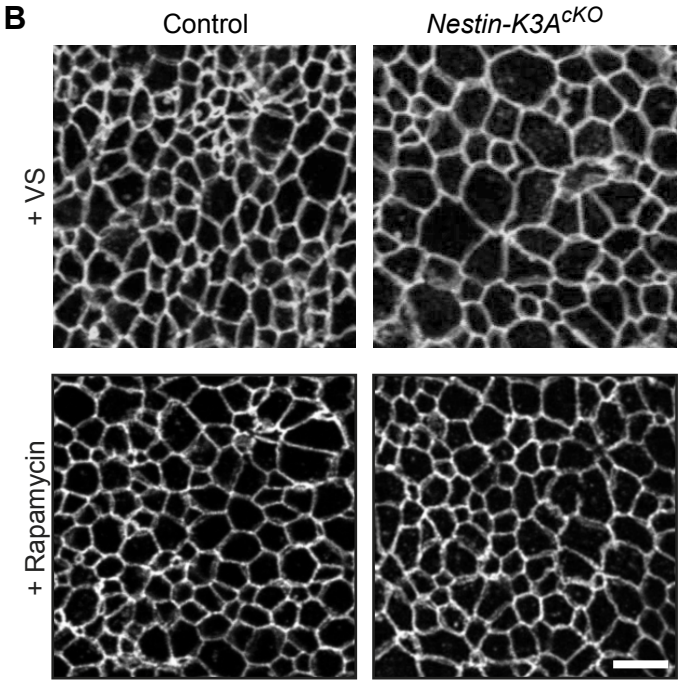

Figure S5: Increased mTORC1 signaling in cilium-less RGC leads to enlargement of the RGC apical domain, which can be rescued by rapamycin treatment. (A) Uncropped images of the western blots shown in Figure 4A. (B) Immunostaining with the ZO-1 antibody of ventricular surfaces on whole mounts of E14.5 control and ciliary mutants injected with vehicle or rapamycin at E12.5. Corresponding segmented images are shown in Figure 4F. Scale bar: 5 µm.

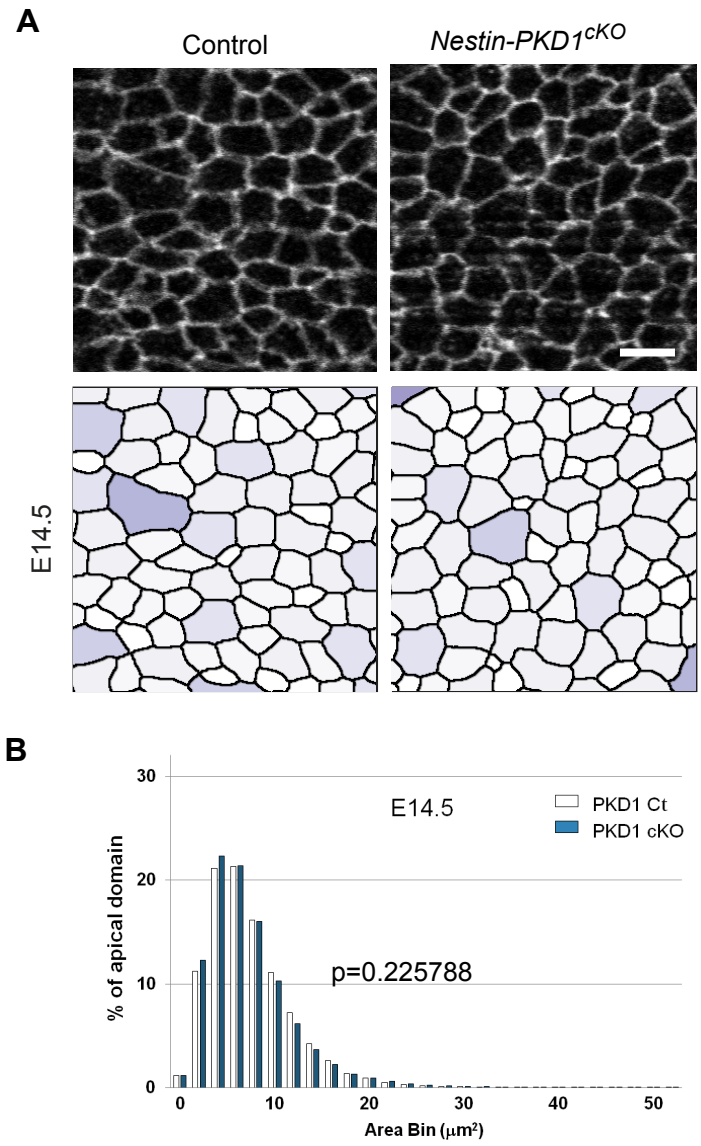

Figure S6: Pkd1 disruption in Nestin-cre derivatives does not lead to enlargement of the RGC apical domain.

(A) Immunostaining with the ZO-1 antibody and corresponding segmented images of ventricular surfaces on whole mounts of an E14.5 control and Pkd1 conditional mutant. (B) Distribution of apical domain surfaces from control (white) and *Nestin-Pkd1*^{cKO} (blue) embryos at E14.5 (2 µm^2 bins). Scale bar: 5 µm.